Heat Capacities of α-Cobalt Sulfate from 5.3 to 300.1 K

Harry E. Bell* and Richard P. Beyer

Thermodynamics Laboratory, Albany Research Center, Bureau of Mines, U.S. Department of the Interior, Albany, Oregon 97321

The heat capacity of α-$CoSO_4$ was determined from 5.3 to 300.1 K by adiabatic calorimetry at the U.S. Bureau of Mines. The values at 298.15 K for $C_p°$, $S°(T) - S°(0)$, $-[G°(T) - H°(0)]/T$, and $H°(T) - H°(0)$ are 103.59, 111.27, 52.92 J·mol^{-1}·K^{-1}, and 17.51 kJ·mol^{-1}, respectively. A λ transition was detected near 10.59 K, attributable to antiferromagnetic ordering.

Introduction

As part of a U.S. Bureau of Mines effort to provide thermodynamic data on minerals and related inorganic compounds, the heat capacity of α-$CoSO_4$ was measured from 5.3 to 300.1 K by adiabatic calorimetry, thereby extending the range of existing measurements below 52 K. The heat capacity of α-$CoSO_4$ was measured previously by Weller (*1*) from 52 to 296 K using an isothermal shield calorimeter.

Experimental Section

Sample Preparation. The sample of α-cobalt sulfate was a very fine powder from the same batch used in Weller's work. The sample was originally prepared by dissolving reagent-grade cobaltous sulfate heptahydrate in water, recrystallizing, and drying (*2*). Since then, the sample has been stored at room temperature in a sealed container under helium atmosphere. Optical emission spectrographic analysis detected the following impurities in parts per million by mass of metal: Cu < 30; Mg < 30; Mn < 300; Ni < 3000. The X-ray powder diffraction spectrum matched that for α-$CoSO_4$ (low-temperature phase, PDF file No. 28-386).

Calorimetric Technique. The automated adiabatic calorimeter used to measure the heat capacities has been described previously by Beyer (*3*). Three series of data were taken with different quantities of sample. Series I covered the temperature range 16.2–300.1 K using a 110.4323-g sample and 1.6 × 10^{-4} mol of helium to increase thermal conductivity. Series II covered the temperature range 10.3–13.55 K using a 93.8853-g sample and 1.7 × 10^{-4} mol of helium. Series III covered the temperature range 5.3–15.7 K using a 73.1074-g sample and 3.6 × 10^{-4} mol of helium. A molecular weight of 154.9908 g·mol^{-1} and a density of 3.857 g·cm^{-3} (for buoyancy correction) were used in the calculations.

Heat capacity determinations were calculated based upon a known input of electrical energy to the sample over a 10-min period. Mean heat capacities were then calculated based on the temperature shift of the sample after thermal equilibration. This temperature shift was normally determined by extrapolating the linear drift rates to the middle of the heating period. Below 10.59 K, long equilibrium periods were encountered due to either helium adsorption or sluggish solid-state transition. In this region equilibration periods of 40 min were used after which the temperature drift curves remained concave upward with drift rates steeper than −5 × 10^{-6} K·s^{-1}. The temperature shift in this case was determined for some data as the difference in temperatures where the drift rate was −6 × 10^{-5} K·s^{-1}; for other data, equilibration periods of over 2 h were used with linear extrapolation of drift rates (see Table I).

Results

The experimental heat capacities are listed chronologically in Table I. The temperature increment for each measurement can be estimated from the proceding and following measurements. Standard deviations about the smooth curve were

Table I. Experimental Heat Capacities of α-$CoSO_4$[a]

T/K	$C_p°$/(J·mol^{-1}·K^{-1})	T/K	$C_p°$/(J·mol^{-1}·K^{-1})
	Series I		Series II
53.69	17.174	10.30	12.669
60.32	21.592	10.48	13.264
63.01	23.318	10.73	11.330
68.29	26.779	10.97	8.040
72.51	29.433	11.27	5.390
83.02	35.733	11.32	4.616
97.78	43.639	11.37	3.960
106.09	47.646	11.43	4.242
114.83	51.551	11.58	3.463
123.65	55.164	11.90	3.419
132.55	58.726	12.18	2.724
141.53	62.079	12.47	2.582
150.56	65.288	12.75	2.414
159.64	68.366	13.02	2.257
168.75	71.289	13.28	2.131
177.89	74.076	13.55	2.050
187.04	76.794		
196.21	79.324		Series III
205.52	81.941	5.88*	1.362
214.85	84.499	6.07*	1.748
223.98	86.816	6.26*	1.785
232.95	89.043	6.46*	2.010
241.75	91.268	6.67*	2.356
250.42	93.296	6.88*	2.598
258.96	95.337	7.09*	3.037
267.38	97.102	7.31*	3.283
275.69	98.888	7.54*	3.554
283.90	100.569	7.77*	3.913
292.03	102.222	8.00*	4.485
300.07	103.789	8.25*	4.697
16.77	1.725	8.50*	5.914
19.20	1.786	8.75*	6.090
21.54	1.999	9.01*	6.940
23.72	2.354	9.28*	8.083
16.24	1.745	9.55*	8.985
17.87	1.737	9.82*	10.663
19.97	1.825	10.39*	14.390
22.11	2.079	10.83	9.791
24.11	2.375	11.81	3.340
25.92	2.898	12.72	2.488
27.89	3.477	13.21	2.368
30.06	4.185	14.19	2.147
32.39	5.052	14.69	2.052
34.90	6.098	15.18	1.984
37.63	7.462	15.68	2.004
40.57	9.045	8.85*	6.130
43.77	10.908	9.12*	6.572
47.24	13.067	9.42*	8.406
50.96	15.430	9.70*	9.466
55.04	18.039	5.33**	0.950
59.52	21.163	5.76**	1.259
64.43	24.139	5.97**	1.398
69.79	27.654	6.16**	1.632
75.67	31.316	6.34**	2.084
82.13	35.193	6.61**	2.317
89.21	39.100	6.97**	2.604
96.98	43.226	8.04**	4.370
105.45	47.364		
114.32	51.369		

[a] * indicates these data were based on temperatures at which the drift rate was −6 × 10^{-5} K·s^{-1}. ** indicates temperature differences based on linearly extrapolated drift rates over time periods greater than 2 h.

Table II. Thermodynamic Functions of α-$CoSO_4$

T/K	$C_p°$/ (J·mol^{-1}·K^{-1})	$\{S°(T) - S°(0)\}$/ (J·mol^{-1}·K^{-1})	$\{-[G°(T) - H°(0)]/T\}$/ (J·mol^{-1}·K^{-1})	$\{H°(T) - H°(0)\}$/ (J·mol^{-1})
0	0	0	0	0
1	0.044	0.042	0.020	0.021
2	0.106	0.090	0.043	0.095
3	0.206	0.150	0.068	0.246
4	0.390	0.232	0.098	0.534
5	0.756	0.353	0.136	1.085
6	1.506	0.549	0.188	2.171
7	2.754	0.873	0.261	4.288
8	4.381	1.339	0.355	7.796
9	6.910	1.990	0.507	13.349
10	10.826	2.906	0.699	22.076
10.59	14.064	3.614	0.840	29.366
11	7.553	4.013	0.952	33.664
12	3.084	4.404	1.226	38.136
13	2.265	4.614	1.480	40.748
14	1.916	4.768	1.709	42.818
15	1.744	4.893	1.917	44.635
16	1.700	5.004	2.107	46.351
20	1.828	5.395	2.726	0.053
25	2.643	5.876	3.307	0.064
30	4.138	6.481	3.783	0.081
35	6.195	7.267	4.222	0.107
40	8.725	8.254	4.663	0.144
45	11.631	9.447	5.126	0.194
50	14.797	10.834	5.626	0.260
60	21.373	14.114	6.759	0.441
70	27.817	17.896	8.075	0.688
80	33.879	22.011	9.557	0.996
90	39.501	26.331	11.179	1.364
100	44.677	30.764	12.915	1.785
110	49.430	35.248	14.742	2.256
120	53.802	39.739	16.638	2.772
130	57.842	44.207	18.587	3.331
140	61.602	48.633	20.575	3.928
150	65.131	53.005	22.592	4.562
160	68.469	57.316	24.628	5.230
170	71.652	61.563	26.676	5.931
180	74.705	65.745	28.730	6.663
190	77.645	69.864	30.787	7.425
200	80.482	73.919	32.843	8.215
210	83.223	77.912	34.894	9.034
220	85.870	81.845	36.939	9.879
230	88.424	85.719	38.976	10.751
240	90.886	89.535	41.003	11.648
250	93.260	93.293	43.020	12.568
260	95.551	96.996	45.025	13.512
270	97.764	100.644	47.017	14.479
273.15	98.446	101.782	47.642	14.788
280	99.903	104.238	48.997	15.468
290	101.967	107.780	50.963	16.477
298.15	103.587	110.629	52.555	17.315
300	103.945	111.271	52.915	17.507

calculated to be 0.6 J·mol^{-1}·K^{-1} below 10.59 K, 0.4 J·mol^{-1}·K^{-1} from 10.59 to 16 K, and less than 0.06 J·mol^{-1}·K^{-1} above 16 K.

A λ transition attributable to antiferromagnetic ordering was found to occur at a temperature of 10.59 K. The nonmagnetic contribution to the specific heat below 40 K was presumed to be of the form $AT^3 + BT$ corresponding to the lattice and lattice dilation components, respectively (*6*). From a linear fit of the data on C_p/T vs. T^2 axes over the temperature range 23–40.6 K it was determined from the y intercept and slope that the lattice dilation contribution to the heat capacity was $0.035\,26T$ and the lattice contribution to the heat capacity was $1.14 \times 10^{-4}T^3$. Subtracting these components from each total heat capacity data point below 23 K gave magnetic heat capacity contributions. The magnetic heat capacities in the vicinity of the critical temperature, 10.59 K, were fitted to an exponential form suggested by Chuang, Schmid, and Chuang (*6*)

$$C_{mag} = T \exp(A + BT)$$

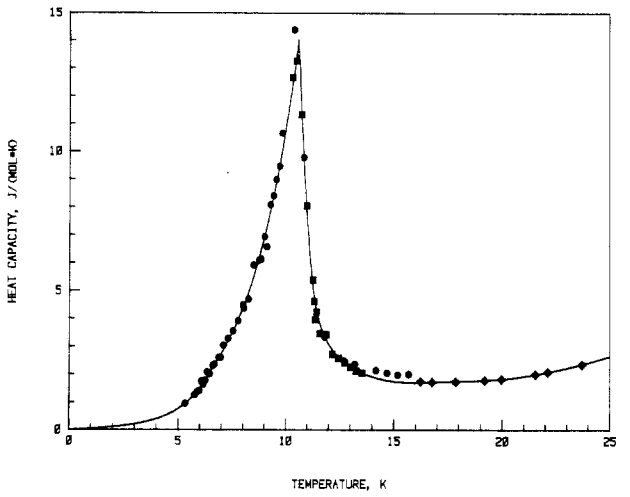

Figure 1. Low-temperature heat capacity of α-$CoSO_4$ to 25 K: ●, series I; ■, series II; ●, series III.

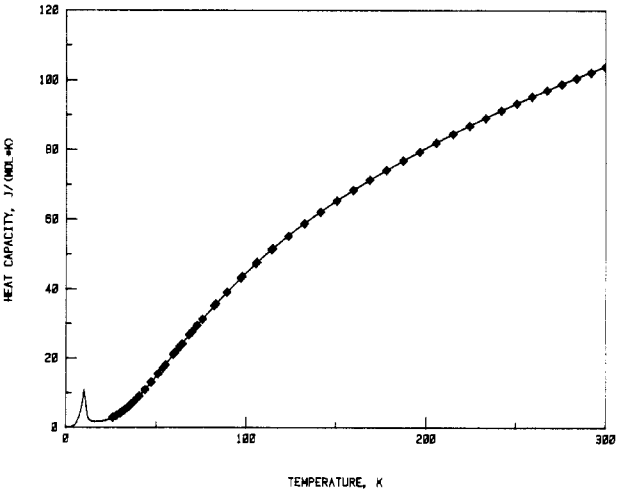

Figure 2. Low-temperature heat capacity of α-$CoSO_4$ to 300 K: ●, series I.

in which A and B are constants found by linear regression of ln (C_{mag}/T) vs. T. Below the critical temperature there appeared to be two distinct curves of this exponential form on either side of ~6.6 K. A linear region of heat capacity from 6.265 to 6.98 K was used to smoothly join the regions on either side. Above the critical temperature the exponential form fit well up to 11.3 K. The temperature range 16–300 K was smoothed by using a least-squares polynomial curve-fitting program developed by Justice (*4*). The temperature range 11.3–16 K was spline-fitted to smoothly join both sides. The data from series III in this latter region appeared incongruous and so were zero weighted. Tabulated thermodynamic functions derived from the above smoothing methods were presented in Table II. Graphs showing the experimental data points as well as the smoothed curve are presented in Figures 1 and 2.

Discussion

The heat capacity curve showed the normal sigmoid shape above 23 K. Comparison of these results with those of Weller (*1*), based on isothermal shield calorimeter measurements over the temperature range 52–296 K, show that his estimate of the absolute entropy of β-$CoSO_4$ at 298.15 K is more than 6% high, assuming no other transitions exist below 5.3 K. The discrepancy can be attributed to his assumption of R ln (4) for the overall magnetic entropy contribution, whereas these data indicate a magnetic entropy contribution of R ln (1.7). Above

52 K, his experimental heat capacity values differ by +0.92% to -0.56% from our smoothed values.

Theory regarding the overall magnetic entropy contribution, S_{mag}, indicates that it should be simply related to the net spin, s, of a compound by

$$S_{mag} = R \ln (2s + 1) \qquad \text{(see Gopal (5))}$$

Our calculated magnetic entropy contribution of R ln (1.7) is close to R ln (2) in agreement with a spin of $^1/_2$.

A crystal field analysis of magnetic susceptibility data for α-$CoSoO_4$ (7) supports this result indicating that an isolated ground Kramer's doublet occurs in this compound.

Acknowledgment

We thank Dr. Hollis Wickman of the Oregon State University Chemistry Department for assisting us in our research of the magnetic behavior of cobaltous compounds.

Registry No. α-$CoSO_4$, 10124-43-3.

Literature Cited

(1) Weller, W. W. *U.S. Bur. Mines, Rep. Invest.* **1965**, 6669.
(2) Adami, L. H.; King, E. G. *U.S. Bur. Mines, Rep. Invest.* **1965**, 6617.
(3) Beyer, R. P.; Ferrante, M. J.; Mrazek, R. V. *J. Chem. Thermodyn.* **1983**, *15*, 827-834.
(4) Justice, B. H. FITAB Program, University of Michigan, Ann Arbor, MI, 1969; COO-1149-143.
(5) Gopal, E. S. R. *Specific Heats at Low Temperatures*; Plenum: New York, 1966; p 98.
(6) Chuang, Y.; Schmid, R.; Chuang, Y. A. *Metall. Trans. A* **1985**, *16A*, 153-165.
(7) Silvera, I. F.; Thornley, J. H. M.; Tinkham, M. *Phys. Rev.* **1964**, *136*, *3A*, A695-A710.

Received for review March 22, 1985. Accepted May 12, 1986.

Wetting Behavior of Molten $PbCl_2$–Alkali-Metal Chloride Mixtures

Torstein A. Utigard, Ding-Chen Mo,† and James M. Toguri*

Department of Metallurgy and Materials Science, University of Toronto, Toronto, Canada M5S-1A4

Contact angles formed on different materials by liquid $PbCl_2$–KCl–NaCl mixtures were measured by using the sessile drop technique. Drop images were obtained on X-ray films by using a high temperature X-ray fluoroscopy unit. Under an argon atmosphere, all chloride mixtures studied formed contact angles less than 40° on substrates of polycrystalline alumina, quartz, and Inconel. Graphite and amorphous carbon substrates were the least wetted, with contact angles between 90 and 150°. Contact angles formed on graphite substrates did not change when the argon atmosphere was replaced with chlorine gas. However, when air was introduced, complete wetting on graphite occurred, probably due to interactions between O^{2-} ions and the graphite substrate.

Introduction

Recently, we determined densities and surface tensions of melts in the $PbCl_2$–KCl–LiCl and $PbCl_2$–KCl–NaCl ternary systems (*1–3*) since these melts were potential electrolytes for the production of metallic lead by electrolysis (*4–6*). During this study, we noted that alkali-metal chloride melts containing $PbCl_2$ tended to creep up the walls of the alumina and silica crucibles. Such an observation suggests that the surface properties of these melts could give rise to problems during electrolysis of $PbCl_2$. In the present note, the contact angles formed by molten lead chloride containing electrolytes on various solid substrates are reported.

Experimental Section

The sessile drop method combined with a high-temperature X-ray fluoroscopy unit was used for contact angle measurements. In this method the image of a liquid drop resting on a horizontal plane surface is required.

The experimental assembly has been described in detail previously (*7*); thus only a brief outline is given. The X-ray beam was generated by a medical-type tube (Picker PX-2A) with a tungsten anode which was rigidly mounted to the furnace bench to avoid changes in alignment. A split graphite resistor furnace containing molybdenum and Inconel radiation shields was used. This furnace assembly was flushed with argon gas which was purified with copper chips at 450 °C to remove oxygen and dried with anhydrous $CaSO_4$. A sessile drop was formed on a horizontal base constructed from the material under study. This sample holder could be rotated up to 90° to allow investigation of the drop symmetry.

Graphite with a density of 1.87 g/cm^3 and an average pore size of approximately 3 μm was used for the present study. Graphite plaques, 3–5 mm thickness, were polished with 1-μm alumina powder to a mirrorlike finish. The Al_2O_3 and ZrO_2 plaques were polished with 1-μm alumina powder. The average alumina grain size was found to be 7 μm. The surface of the ZrO_2 showed presence of small cracks. These cracks were on average 2–3 mm long and about 0.1 mm wide.

The required amounts of reagent-grade salts were mixed together and heated to 150 °C under vacuum (1 kPa) for 20 h to remove moisture. The salt mixture was then melted under a chlorine atmosphere. After chlorine gas bubbling, purified argon gas was bubbled through the melt for 1–2 h to remove any dissolved chlorine. A polished plaque was placed inside the sample holder and the purified premelted salt mixture was placed on the center part of the plaque. The sample holder was placed inside the reaction tube which was evacuated and flushed with argon. The sample assembly was then heated to the required temperature. As shown in Figure 1, one thermocouple was placed above the sessile drop and another below. The temperature difference between these thermocouples was 5 K.

Results and Discussion

The results of the contact angle measurements are summarized in Tables I and II. Substrates made of polycrystalline alumina (Al_2O_3), quartz (SiO_2), and Inconel were all wetted with contact angles less than 40° by all the liquids investigated as shown in Table I. The measurements were carried out under an argon atmosphere and up to about 100 K above the melting

† Present address: Central-South Institute of Mining and Metallurgy, Changsha, Hunan, China.

0021-9568/86/1731-0383$01.50/0